New constraints on the long-term debris-flow incision law based on high resolution topographic data

Aude Lurin, Odin Marc, Sebastien Carretier, Patrick Meunier

New constraints on the long-term debris-flow incision law based on high resolution topographic data

A. Lurin[1], O. Marc[1], S. Carretier[1], P. Meunier[2]

[1]GET, Université de Toulouse, CNES, CNRS, IRD, UPS, Toulouse, France
[2]Laboratoire de Géologie de l'Ecole Normale Supérieure, Paris, France

Key Points:

- With a novel method we extract gradient and concavity of all first-order channels from 38 mountain catchments with meter-scale topography
- Slope gradient scales non-linearly with ^{10}Be erosion rate and concavity remain stable near 0.1, across a range of rock-type and climate
- Our results support an updated debris-flow incision model linking flow mass and sediment delivery, and newly constrain 3 key parameters

Corresponding author: Aude Lurin, aude.lurin@get.omp.eu

Abstract

In spite of recent development, state-of-the-art debris-flow incision models (DFIM) remain under-constrained, limiting their integration in landscape evolution model (LEM), and thus our understanding of catchment erosion dynamics, including their altitude distribution, their response to climatic and tectonic changes and drainage network reorganization. Here, we use a novel method to extract channel heads on high-resolution topographies of 38 catchments spanning two orders of magnitude of erosion rates, and constrain the gradient and concavity of hundreds of first order-channels. We show that this is consistent with a novel, refined analytical DFIM prediction and constrain the exponents relating incision E_{df}, slope gradient S_{ch} and debris-flow thickness H: $E_{df} \propto S_{ch}^{4.2\pm0.9} H^{0.8\pm0.6}$. We also provide constraints on the range of possible value for debris-flow erodibility, as a function of debris-flow frequency, and suggest further analysis on channel junctions and concavity. These results pave the way to an implementation of a DFIM in 2D-LEMs.

Plain Language Summary

Our understanding of the long-term coupling between climate and tectonics activity and their effect on mountain building and sediment production and export is mediated by the use landscape evolution model, mathematical models describing the competition between rock uplift and erosion processes. In spite of recent development,erosion caused by debris flows remains too under-constrained to be included in LEM. Here, we use a novel method to extract channel heads on high-resolution topographies of 38 catchments spanning two orders of magnitude of erosion rates, and constrain the morphology of channels in their initial reaches. We show that this morphologies match the prediction of an improved debris-flow incision model and constrain the exponents modulating the dependency of erosion on slope gradient and debris-flow thickness. We also provide constraints on the range of possible value for debris-flow erodibility, as a function of debris-flow frequency, another key parameter of this model, which open the way to an implementation of this debris-flow incision model in LEMs.

1 Introduction

By transforming bedrock into sediments and routing them throughout entire continent, erosion and transport processes play a significant part in Earth's dynamic, including its climate. Quantifying these processes and modelling them in landscapes evolution models (LEMs) is therefore a necessary step for exploring diverse questions in geosciences such as the role of climate and tectonics in driving mountain uplift (Molnar & England, 1990), the controls on mountain ranges altitude (Whipple et al., 1999; Egholm et al., 2013), the global cycles of various elements including carbon (France-Lanord & Derry, 1997). While the first LEMs only considered basic fluvial incision and hillslope diffusion (Kooi & Beaumont, 1996), newer ones can include more refined details such as unsteady overland water flow (Davy et al., 2017), stochastic landsliding (Densmore et al., 1998; Campforts et al., 2020) or clast tracking (Carretier et al., 2016), allowing for a finer representation of landscape dynamics. However, debris flows remain missing in LEMs even if they may dominate incision and morphology in upstream mountain channels (Stock & Dietrich, 2003; Hergarten et al., 2016; Neely & DiBiase, 2023). This imply potential bias in representing head water catchment dynamics, which might control drainage network reorganisation and ridge migration (Mudd & Furbish, 2005; Willett et al., 2014), mountain elevation (Whipple et al., 1999) or sediment fluxes changes in response to tectonic or climatic changes (Benda & Dunne, 1997). Preliminary studies have proposed a debris-flow incision model (DFIM) at the event scale (Hsu et al., 2008; McCoy, 2012) and its consequences for channel longitudinal profile (Stock & Dietrich, 2006). More recently McGuire et al. (2023) presented a relatively parsimonious DFIM able to reproduce the transition from constant slope colluvial channel to concave fluvial chan-

nel observed in the field (Stock & Dietrich, 2003; DiBiase et al., 2010; Struble et al., 2023). This DFIM essentially relies on a non-linear scaling between erosion rate E, debris-flow erodibility and thickness, k_{df} and H, and the local slope gradient, $E \propto k_{df} S^{\alpha} H^{\beta}$, as initially proposed by McCoy (2012). But for now, k_{df}, α and β are largely under-constrained, limiting DFIM insights and implementation in 2D-LEMs.
Past developments of LEMs have especially been made possible by the use of topographic data for characterizing the shape of landscapes. Relationship between slope gradient and drainage area reflect the balance between the erosive power of erosion processes and tectonic uplift (Tucker & Bras, 1998; Tucker & Hancock, 2010). For instance, the characterization of the slope/area relationship of fluvial channels and the measurement of knickpoint migration rate, together with physics-based developments, has allowed to constrain the fluvial stream-power incision model (Lague, 2014). Nevertheless, the low resolution of former topographic data limited the analysis of debris-flow dominated portions of the landscape. In particular, defining where debris-flow channels begin has long been a problem in geomorphology (Montgomery & Dietrich, 1988). New possibilities were opened by airborne LiDAR digital elevation models(DEMs) providing meter scale resolution, and revealed that channels experiencing debris-flow incision exhibit a distinct slope/area relationship from fluvial channels Stock and Dietrich (2003). In the last years a few more studies combined high-resolution DEMs and ^{10}Be-derived erosion rates with the goals to understand more precisely how debris-flows control channel shape and ultimately to connect it with candidate DFIM. In the San Gabriel (SG) and San Jacinto (SJ) mountains and the Oregon Coast range, the drainage area of transition from near constant gradient associated with debris-flow to concave fluvial channel was observed to increase with erosion rates (DiBiase et al., 2012; Penserini et al., 2017; Neely & DiBiase, 2023). Though some studies initially thought the characteristic gradient of these channels was uncorrelated to erosion rates (Penserini et al., 2017) recent studies found a weak but clear increase of channel gradient with erosion rates, both in the SG, and a compilation of US catchments (Struble et al., 2023; Neely & DiBiase, 2023). Further, Struble et al. (2023) showed that these correlations between morphology and erosion rates could be reproduced to first-order by the 1D-LEMs combining a DFIM and SPIM (McGuire et al., 2023). Various combinations of parameters were equivalent in fitting the data as long as they respected $\alpha > 3\beta$ and we do not know how the DFIM parameters may vary with lithology or climate. Additionally, it was suggested that the upstream channel slope gradient may decouple from erosion rates, based on a US data compilation (Neely & DiBiase, 2023), a trend potentially existing in the SG data too but not consistent with the DFIM (Struble et al., 2023).
However, a common issue of all morphometric analysis until now is that they (i) used diverse, unjustified definition of the upstream channel boundary, and (ii) fitted the empirical framework of Stock and Dietrich (2003) to the bulk catchment slope-area data to derive debris-flow metrics, even though it is not consistent with existing DFIM. To address these two challenges we propose to individually extract all first-order channels from a compilation of 38 catchments with known erosion rates, thanks to a novel method allowing to identify channel heads in the colluvial domain (Lurin et al., 2023) and to compare their average morphology to direct prediction from an updated DFIM. Thus, we obtain unprecedented constraints on several key parameters of the DFIM opening new opportunities for the inclusion of DFIM into 2D-LEMs.

2 Analytical model of the slope gradient in channels carved by debris-flow incision

Here, we focus on first-order channel immediately downstream channel heads, thus neglecting fluvial erosion and the threshold factor reflecting a reduction in incision when debris flows approach rest. Therefore we can write the debris-flow erosion rate, as a function of slope gradient S and debris-flow depth H:

$$E_{df} = k_{df} F_{df} t_p S^{\alpha} H^{\beta} \tag{1}$$

With t_p the time of passage, k_{df} an erodibility coefficient depending on bedrock and flow properties, F_{df} the debris flow frequency, and α and β scaling exponent (McGuire et al., 2023). Combining empirical laws relating debris-flow volume, M, peak discharge and velocity as found by Rickenmann (1999), mass conservation and a channel width scaling with drainage area (i.e., $w = k_w A^b$), Equation 1 can be reformulated as a function of A mainly (McGuire et al., 2023). Thus, assuming steady-state, it allows to express channel slope gradient as a function of U and A.
However, in contrast to McGuire et al. (2023) we assume that, in first-order channels each debris flow transport all sediment previously delivered by hillslopes, consistent with *en-masse* failure at high gradient and low drainage (Prancevic et al., 2014; DiBiase & Lamb, 2019). This implies, from mass conservation, that we have $M = \frac{UA}{f_s F_{df}}$ with f_s the sediment fraction of the flow. With these assumptions, we derive an expression for debris-flow first-order channel slope gradient, S_{ch}:

$$S_{ch} = K^{-\frac{\beta}{3\alpha-\beta}} k_{df}^{-\frac{3}{3\alpha-\beta}} \left(\frac{U}{F_{df}}\right)^{\frac{c_2(3-\beta)}{3\alpha-\beta}} A_{ch}^{-\frac{3(1-c_2)+(c2-b)\beta}{3\alpha-\beta}} \tag{2}$$

Where $c_2 = 0.8 \pm 0.05$ is an empirical exponent scaling debris-flow discharge with volume constrained by the literature Rickenmann (1999), $b = 0.2 \pm 0.1$ for upstream bedrock channels (DiBiase & Whipple, 2011; McGuire et al., 2023; Neely & DiBiase, 2023), and K is a combination of parameters involved in characterizing debris-flow erosion, velocity, discharge, channel width analogous to the one for SPIM (Lague, 2014; DiBiase & Whipple, 2011) (See supplementary information for a full derivation).
Equation 2 suggest that α and β have a determining impact on the way uplift, debris-flow-frequency and drainage area control channel slope. It defines a concavity for debris-flow channels:

$$\theta_{df} = \frac{3(1-c_2) + \beta(c_2 - b)}{3\alpha - \beta} \tag{3}$$

and it predicts a power-law scaling between S_{ch} and uplift, or erosion rate at steady-state with an exponent e_U:

$$e_U = \frac{c_2(3-\beta)}{3\alpha - \beta} \tag{4}$$

This model also suggests that detailed analysis of debris-flow channel slope and concavity in natural catchments may provide strong constraints on these two parameters.

3 Compilation of steady-state catchments with known erosion rates and high-resolution DEM

To constrain the analytical model presented above we need accurate constraints both on the first-order channel topography and on the steady-state catchment-average erosion rate. Thus we limit our analysis to catchments with (i) available 1-m resolution LiDAR digital elevation models (DEMs), (ii) available ^{10}Be denudation rate measurements and (iii) evidence of steady-state topography without glacial overprinting in the headwaters were we find first order channels (Table 1). Indeed, inclusion of criteria (iii) removed many catchments with glacial topography in the French and Swiss Alps, or basins from the Feather river reported by (Hurst et al., 2013) which are undergoing transient readjustment. Further, we compute Chi-Z plots for each basins and rejected a number of basins (from DiBiase et al. (2010, 2012)) with deviations from linearity and large disorder metrics which suggest some type of drainage reorganisation or transient dynamics (Perron & Royden, 2013; Hergarten et al., 2016). As a result of this selection, we focus on 38 basins in four different mountain range, the San Bernardino (SB) and San Gabriel (SG) mountains, the Oregon Coast (OC) range and the Valensole Plateau (VP) in France (Table 1). These basins have different erosion rates ranging from about 0,03 mm/yr to 3 mm/yr, and were derived from the same method (Mudd et al., 2016), as reported in the Octopus database (Codilean et al., 2022). Data from DiBiase et al. (2012) is not in

Table 1. Information about the studied basins. References: (Binnie et al., 2007; DiBiase et al., 2012; Marshall et al., 2017; Penserini et al., 2017; Godard et al., 2020) for B07, D10, D12, P17 and G20, respectively, with basin code from source. Erosion rates are from the Octopus database except for the references with a *. θ and S_{ch} values are median values from all 1st order channels extracted in the basin, while 25th and 75th percentiles are in supplement. Abbreviation for range and lithology: SG: San Gabriel; SB: San Bernardino; OC: Oregon Coast; VP: Valensole Plateau. C/ Crystalline basement; T: Turbiditic sedimentary rocks; Co: Clast-supported conglomerate; MAP: Mean Annual precipitation, as reported in Neely and DiBiase (2023) for US sites and Godard et al. (2020) for VP.

Code	Ref	E (mm/yr)	1σ (mm/yr)	Area (km²)	Channels	θ	S_{ch}	Range / Litho / MAP (m/yr)
SGB5	D10	0.1464	0.041	9.9	563	0.14	0.69	SG / C / 0.6-1.3
SGB9	D10	0.448	0.093	17.3	424	0.07	0.51	SG / C / 0.6-1.3
SGB6	D10	0.267	0.149	9.7	408	0.13	0.70	SG / C / 0.6-1.3
SG123	D10	0.099	0.02	3.2	97	0.07	0.47	SG / C / 0.6-1.3
SG206	D10	0.278	0.103	5.4	175	0.05	0.73	SG / C / 0.6-1.3
SG207	D10	0.253	0.058	6.5	313	0.04	0.72	SG / C / 0.6-1.3
SG140	D10	0.182	0.039	7.7	0	0.00	0.00	SG / C / 0.6-1.3
SG0809	D12*	0.434	0.059	3.8	158	0.08	0.74	SG / C / 0.6-1.3
SG0804	D12*	0.493	0.111	2.5	98	0.13	0.74	SG / C / 0.6-1.3
SG0805	D12*	0.343	0.058	3.2	98	0.07	0.58	SG / C / 0.6-1.3
SGB10	D12*	0.279	0.023	3.0	185	0.10	0.63	SG / C / 0.6-1.3
SG126	D12*	0.591	0.071	2.3	122	0.00	0.82	SG / C / 0.6-1.3
SG125	D12*	0.465	0.061	2.0	89	0.08	0.77	SG / C / 0.6-1.3
SG818	D12*	0.711	0.13	2.0	132	0.18	0.71	SG / C / 0.6-1.3
SGB7	D12*	0.253	0.054	2.3	133	0.09	0.72	SG / C / 0.6-1.3
SG0704	D12*	0.668	0.186	2.1	106	0.04	0.67	SG / C / 0.6-1.3
SGB2/SG124	D12*	0.15	0.05	3.8	225	0.17	0.43	SG / C / 0.6-1.3
SG0748	D12*	0.541	0.147	2.0	117	0.11	0.72	SG / C / 0.6-1.3
SG127	D12*	0.736	0.099	2.3	143	0.06	0.82	SG / C / 0.6-1.3
SG151/SG152	D12*	0.256	0.18	2.0	49	0.04	0.54	SG / C / 0.6-1.3
SG0708	D12*	0.435	0.068	1.9	94	0.08	0.66	SG / C / 0.6-1.3
SG0749	D12*	0.611	0.195	2.6	109	0.07	0.77	SG / C / 0.6-1.3
CRN503	P17	0.087	0.021	18.2	438	0.06	0.69	OC / T / 2.1-2.3
HadsCRN	P17	0.111	0.03	1.8	79	0.06	0.63	OC / T / 2.1-2.3
Trib1	M17	0.078	0.02	0.7	20	0.15	0.51	OC / T / 2.1-2.3
Trib2	M17	0.055	0.014	0.3	10	0.01	0.68	OC / T / 2.1-2.3
CRN501	P17	0.072	0.041	2.0	85	0.10	0.56	OC / T / 2.1-2.3
CRN502	P17	0.067	0.017	0.7	34	0.06	0.51	OC / T / 2.1-2.3
CRN500	P17	0.059	0.013	2.0	83	0.04	0.50	OC / T / 2.1-2.3
Bin-1	B07	1.94	0.54	1.1	30	0.09	0.64	SB / C / 0.6-0.8
Bin-2	B07	2.8	0.764	0.6	28	0.19	0.76	SB / C / 0.6-0.8
Bin-3	B07	1.176	0.257	2.4	119	0.11	0.85	SB / C / 0.6-0.8
Bin-4	B07	1.032	0.223	0.9	76	0.15	0.85	SB / C / 0.6-0.8
Bin-5	B07	1.134	0.254	0.3	24	0.14	0.89	SB / C / 0.6-0.8
Va-19-K	G20*	0.05	0.02	3.5	68	0.10	0.34	VP / Co / 0.7
Va-18-G	G20*	0.05	0.02	2.4	58	0.01	0.24	VP / Co / 0.7
Va-15-M	G20*	0.045	0.018	1.5	27	0.11	0.16	VP / Co / 0.7
Va-13-ON	G20*	0.03	0.012	1.4	49	0.19	0.29	VP / Co / 0.7

this database but followed a similar method and rates reported by DiBiase et al. (2010) with the same method are within 10% of their Octopus counterpart. For VP the erosion rates is not the results of a sand sample at the basin outlet, but of in-situ hillslope denudation rates converted to a basin estimates through an extraction of hilltop curvature (Roering et al., 2007; Hurst et al., 2013) and their variability derive from variability in hilltop curvature.

The sites represent diverse climatic and lithological conditions. SB and SM have a dry Mediterranean climate with sparse vegetation and lie on crystalline basement (weathered granite). VP has a similar Mediterranean climate with slightly more developed vegetation and lie on young, gravelly conglomerate. OC has about twice more precipitation, with developed coniferous forest over most slopes and lie over turbidite sequence with siltstone and sandstone. In addition, direct field evidence of debris-flow activity and incision in their upstream channel area exist for several selected catchments in the Oregon Coast range and the San Gabriel and San Bernardino mountains (Stock & Dietrich, 2003; Kean et al., 2011, 2013; DiBiase & Lamb, 2019).

4 Methods

We use the Matlab TopoToolbox to analyse the topographic data (Schwanghart & Scherler, 2014). In order to reduce meter-scale irregularities, we applied a Wiener filter on the DEMs. In contrast to previous studies, instead of extracting the bulk statistics of slope gradient at low drainage area (DiBiase et al., 2012; Struble et al., 2023; Neely & DiBiase, 2023) we extract independently the slope gradient of individual first order channels and then analyze their statistics.

4.1 Retrieving the channelized domain

Debris-flow channels are the most upstream channels in a catchment. In order to study the first order debris-flow channels, we thus have to retrieve channel heads. Several automatic methods exist for automatically extracting channel heads from high resolution topographic data. We use the CO^2CHAIN method (Lurin et al., 2023), which was developed specifically for high erosion-rate DEMs and was shown to work well on catchments with diverse topography and erosion-rates, without needing recalibration. After retrieving the localization of channel heads, we use a D8 routing algorithm to extract the whole channel network. Depending on catchment size, we retrieved from a few dozens to a few hundreds first-order channels (Table 1), allowing to derive significant statistics on S_{ch}. In each basin, 75% of the first-order channels maximal drainage area is below 10,000 and 30,000 m^2 which we take as a sign that overall all the topographic analysis are mostly upstream of the transition toward channel with a "large concavity" ($> 0.3 - 0.5$) considered dominated by fluvial processes landscape, typically between 0.1 and 1 km^2 in the studied regions (Neely & DiBiase, 2023).

4.2 Analysing slope gradient within first-order channels

For each catchment, we retrieve the initial slope of the debris-flow domain, i.e. the slope at channel heads, as well as the concavity of first-order debris-flow channels.

Slope measurement is greatly affected by local, meter-scale irregularities which can reflect the presence of boulders, local heterogeneities in the bedrock or tree uprooting. We consider the resulting slope variations as not representative of the long-term effect of debris-flow erosion. Therefore, we need to calculate slope at a scale which smooths these variations without erasing actual long term slope variations. We found that averaging slope over a 7 m moving window along the channel flowpath greatly reduced pixel-to-pixel slope variation without smoothing too much the channel profile (Penserini et al., 2017).

In order to calculate the concavity θ of single channel segments, we consider the following relationship between slope S and drainage area A:

$$S = S_0 A^{-\theta}$$

Therefore, we perform a linear regression between the logarithm of slope and drainage area to retrieve the concavity. Both for concavity and channel gradient we compute the median, 25th and 75th percentile of the distribution of each catchment.

5 Results

5.1 Initial slope of the debris-flow channels

Given that gradient jointly depend on E and A, we used the median value of concavity for each catchment and corrected the slopes found at channel heads to compute the expected gradient at $A = 10^4\ m^2$. The normalized median of initial gradient increases with the erosion rate E (Figure 1a). Ignoring the four VP basins which seem to deviate from the main trend, we performed a bootstrapped linear regression on the logarithm values of S_{ch} and E, producing 50 samples of 34 $E-S$ pairs, randomly drawn with replacement from our dataset, and yielding:

$$S_{ch} = (0.78 \pm 0.03)E^{0.15\pm0.03}$$

with $R^2 = 0.54$ ($N = 34$).

5.2 First-order channel concavity

We found median concavities slightly above zero for most catchments (Figure 1b). Despite smoothing gradient along the channels, concavities distribution remain broad with a number of convex channels (steepening downstream) and interquartile ranges typically between 0.4 and 0.6 and apparently growing towards lower erosion rates most found in VP and OC catchments. Nevertheless, we do not observe a significant trend with erosion rate, and the average of median concavities from the 38 catchment seems well constrained with $\bar{\theta_{df}} = 0.09 \pm 0.009$ (standard error of the mean with a standard deviation $\sigma = 0.05$).

5.3 Constraints on α, β and k_{df}

Our topographic analysis provides strong constraints on θ_{df} and e_U (Figure 1), which, together with literature constraints on b and c_2 constrain the possible value range for α and β (Figure 2 and Supplement for equations). Assuming uncorrelated, normal uncertainties we derive a best estimates with 1σ uncertainties of $\alpha = 4.2 \pm 0.9$ and $\beta = 0.8 \pm 0.6$. The uncertainties are dominated by uncertainties on θ_{df} and we may derive a lower uncertainty range, $\alpha = 4.2 \pm 0.5$ and $\beta = 0.8 \pm 0.3$, if we assume that uncertainties on β and α only derive from the uncertainties on the mean concavity $\bar{\theta_{df}}$. This implicitly assumes that the variability of θ_{df}, within and between catchments (Figure 1), is not related to variations on α and β but to other aspects, such as fine-scale variability of c_2 and b, or measurement errors (from the DEM, the channel head identification or the extraction methods).

With these refined constraints on α and β and using typical values for the other physical and empirical parameters, as in McGuire et al. (2023) (see Supplementary for a full description), we may also derive constraints on two essential parameters of the debris-flow incision model, k_{df} and F_{df} (Eq 2, Figure 2b). Unsurprisingly we found a trade-off in which the best estimate of k_{df} (i.e., when $\alpha = 4.2$ and $\beta = 0.8$) decreases from about 1 to 0.1 $m^{1-\beta}.s^{-1}$ as F_{df} increases from 10^{-3} to 10^{-1} yr^{-1}. However, uncertainties remain very large ($>$ 2 order of magnitudes) if we consider the range of possible values for α and β. Indeed, k_{df} tends to be proportional to $1/F_{df}$ when $\beta -> 0$ and also increases with decreasing α (See Supplementary). Again, if we limit uncertainty to the mean concavity $\bar{\theta}$ and the propagated uncertainties shrink (Figure 2b).

6 Discussion

Before discussing our results in terms of channel morphology and implications for debris flow incision model (DFIM), we stress that the variability observed for different metrics may in part be due to the stochastic nature of debris-flow erosion. Indeed, even in a steady-state catchment, the (unknown) distribution of properties and timing of recent debris-flow may vary from channel to channel, leading to potential fluctuation of the morphometry around a mean prediction. Correlating morphometric variability to debris-flow history is a future research challenge beyond the scope of this study.

6.1 Slope and concavity of debris-flow channels

The relationship we found between initial slope and erosion rate is consistent with the latest studies conducted about debris-flow channels slope. While previous studies con-

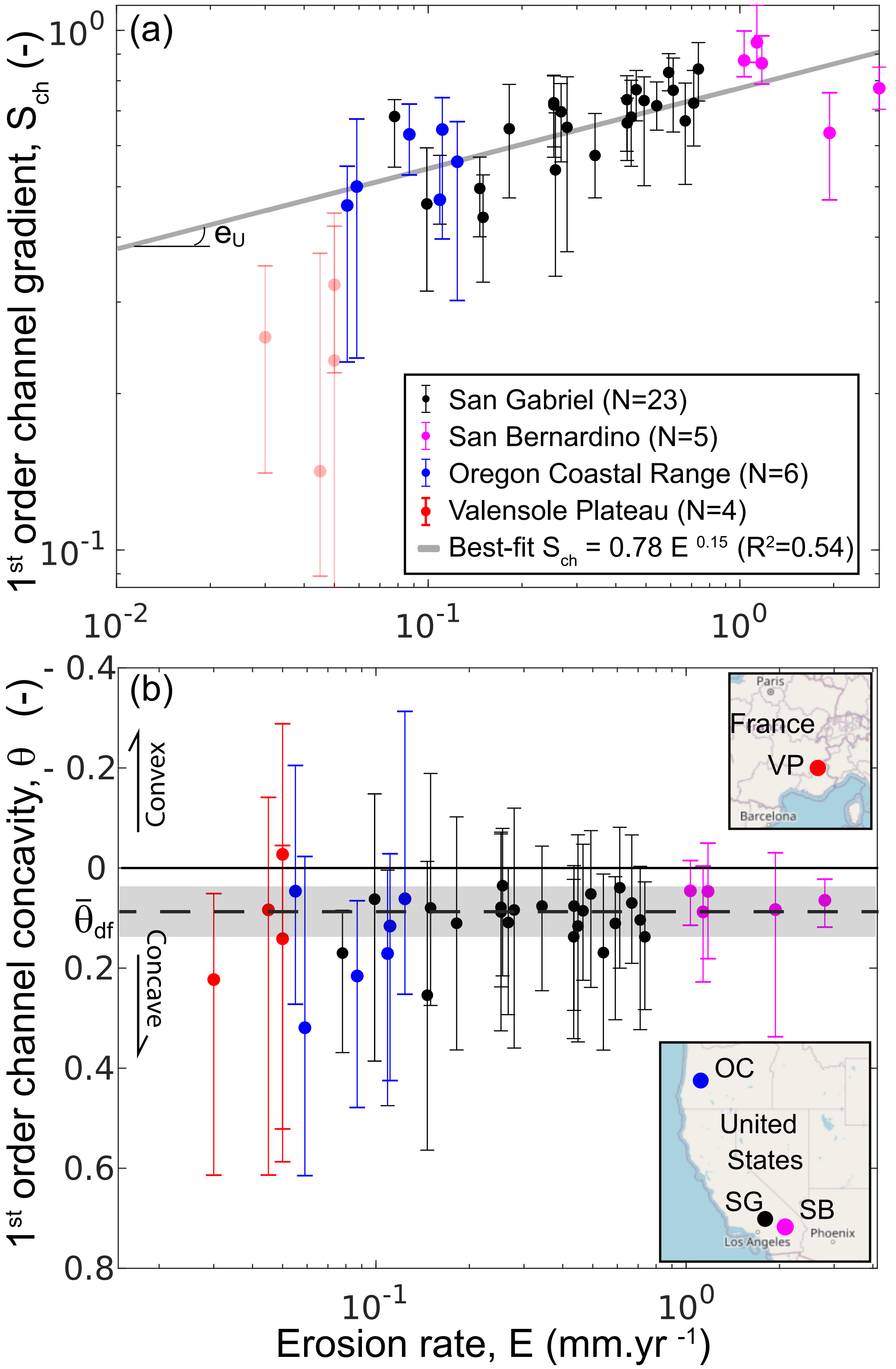

Figure 1. (a): Slope gradient of first-order channels (normalized at $A = 10^4\ m^2$) against erosion rate. (b): Concavity of first-order channels against of erosion rate. Dashed line and grey zone represent the mean concavity and 1σ range. Points with whiskers represent the median, and 25-75th percentiles of the distribution of all channels within basins color-coded by geographical areas. Insets show the location of the four geographical areas.

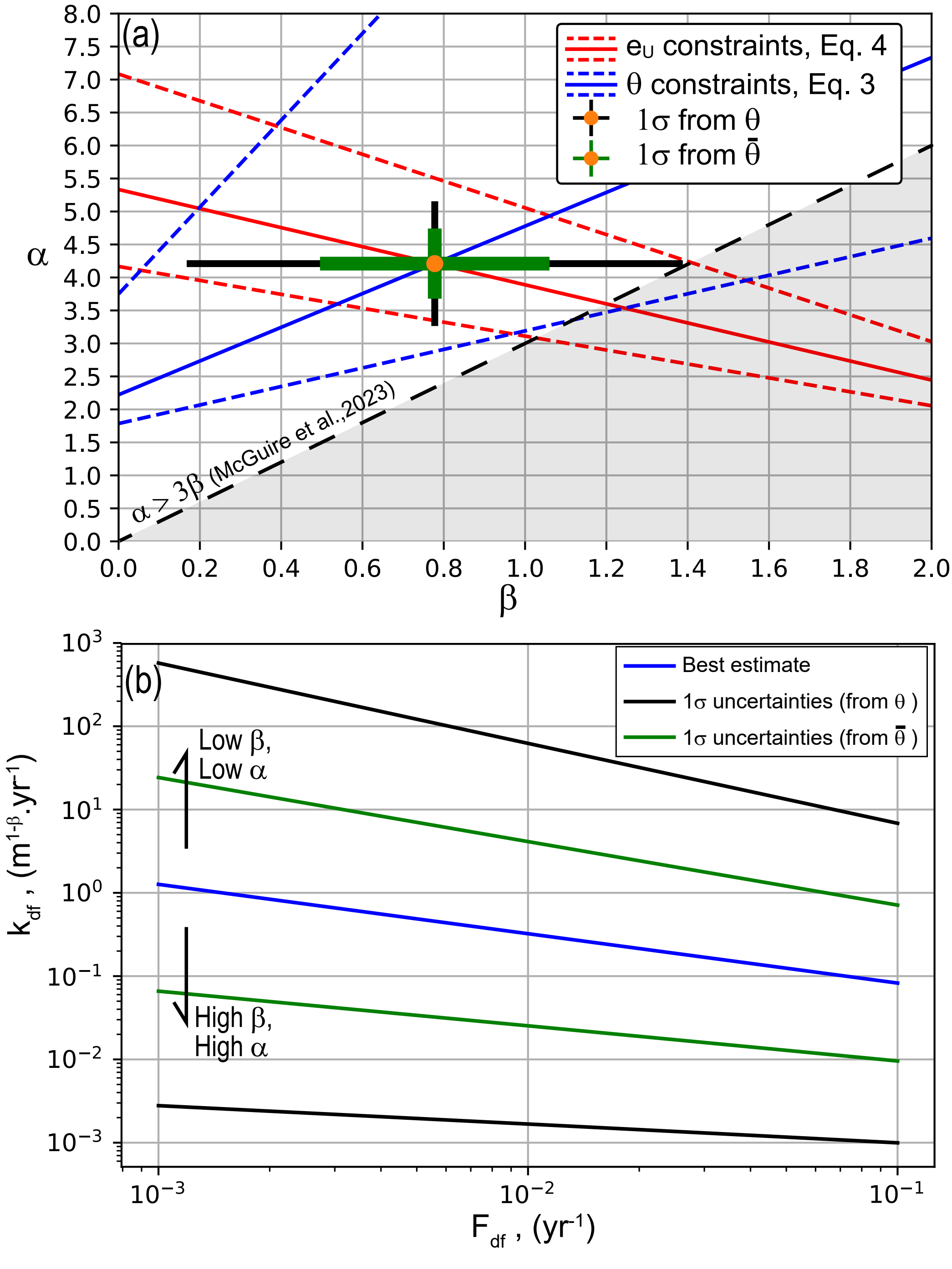

Figure 2. (a): Range of possible values for the α and β scaling exponents. Blue and red dashed lines are range of possible values when considering uncertainty range from the S-E scaling and concavity respectively. Black and green error bar are the 1σ uncertainties derived from Gaussian error propagation from variability on θ or $bar\theta$. Dashed line and grey zone show the only pre-existing constraints before this study. (b): Range of possible values for K_{df} as a function of the debris-flow frequency, F_{df}, with error propagated from (a).

sidered the initial slope of debris-flow channels to be controlled by the threshold slope of hillslopes and therefore relatively independent on erosion rate (DiBiase et al., 2010; Penserini et al., 2017), recent work found a positive correlation between upstream channel slope gradient and erosion rate (Struble et al., 2023; Neely & DiBiase, 2023). Struble et al. (2023) relationship between slope and erosion rate, obtained by fitting empirical debris flow scaling (Stock & Dietrich, 2003), to binned slope-area data from whole catchments in the San Gabriels Mountains is nearly the same as ours. However, our approach allowed a substantial scatter reduction and extended this result to a broader range of erosion rate and to other lithological and climatic settings. Indeed, our extended database demonstrate that the Oregon Coast Range and San Bernardinos Mountains catchments follow the same trend, in spite of different lithology and climate, especially for Oregon. Based on data over several geographical zones, partly shared with our dataset, Neely and DiBiase (2023) proposed that debris-flow gradient could saturate near 0.8 above $E > 0.3\ mm.yr^{-1}$. Although less scattered (Figure S1) and more strictly selected, our dataset cannot completely disprove this alternative approach, given that the analytical DFIM predicts a weak power-law increase, and that small deviation for the two SB basins with the highest erosion rates may suggest saturation. Saturation may also reflect the inability of debris flows to compete with hillslope processes such as landsliding, as suggested by the observation that S_{ch} converge toward the mean hillslope gradient at high erosion rates (Figure S2). To distinguish these interpretations we suggest more analysis at high erosion rates ($\sim 1mm/yr$) and further attempts to understand the variability of S_{ch}.

As for the concavity of debris-flow channels, it has rarely been looked at (Lague & Davy, 2003), and recent studies on debris flow used the framework proposed by Stock and Dietrich (2003) which transition from fluvial concavity towards a null concavity at small drainage area. Interestingly, the concavity we found in the very first channel reaches is not null, and is quite consistent across two orders of magnitude of erosion rates and rather different environmental conditions (Figure 1). We recognize that measuring concavity at the scale of one single $\sim$ 100m long channel is difficult and that some of the intra-basin dispersion may be measurement errors (Figure 1(b)). Alternatively, part of the dispersion may also reflect local variability of controlling factors of the concavity, such as c_2 the volume-discharge scaling for debris flow, or b the channel width exponent. However, the weak variations of the mean suggest that if these variations exist they remain around a fairly consistent mean, rather independent of uplift rate, climate and vegetation. Another aspect meriting further research are the convex channels with $\theta < 0$ that, if correctly measured, would suggest unusual values for c_2 and b (e.g., $b > c_2$) or suggest that debris-volume do not grow linearly with A which may lead to initially convex channel (McGuire et al., 2023).

In contrast, the Valensole Plateau catchments appear to depart from the $E{-}S_{ch}$ scaling, where they have a less steep gradient than other catchments. Nevertheless, concavity in VP appears consistent with the other catchments (Figure 1). Given that there is no documented debris-flow activity in these catchments, we cannot exclude that the low concavity of first order channels may result from other processes. For example in this catchment, sapping might be an important part of channel initiation and carving (Berhanu et al., 2012). Alternatively, the lower S_{ch} but similar concavity observed in Valensole catchments, may be due to a steady state driven by debris-flow incision with a higher value for debris-flow erodibility k_{df} or debris flow frequency, F_{df} than in the other basins. Given the weakly consolidated conglomerate, a higher debris-flow erodibility would be unsurprising in these catchments.

6.2 Constraints on the debris-flow incision law

Our results are extending the analytical model developed by McGuire et al. (2023), modified here to consider that all sediments are moved by debris flows and to explicitly distinguish the role of debris-flow frequency and erodibility. We have shown that the morphometry of first-order channel of catchments in various conditions appeared consistent with our updated DFIM (Eq 2) and yielded unprecedented constrains on the model exponent. Preliminary modeling could suggest $\alpha > 1$ and $\beta < 1$ (McCoy, 2012), while further modeling and comparison with data clarified that $\alpha/\beta > 3 - 5$ (McGuire et al., 2023; Struble et al., 2023), but still considered very broad range of values typically $2 < \alpha < 8$ and $0.5 < \beta < 2$, and left untested values of $\beta < 0.5$. Although we do find a value of β near one and with a rather large range, including values below 0.5, we considerably narrow the possibility for α, and suggest $3 < \alpha < 5$.

Since debris-flow height is closely related to volume, the value of β controls whether several debris-flows are more or less incising than a single debris flow with equivalent total volume. Our model predict that as long as $beta < 3$, S_{ch} will increase with uplift rate (Fig 1) and thus will decrease with increasing debris-flow frequency, suggesting that frequent, small debris flows are more efficient than rare, large ones. Additionally, a potential way to further constrain β could be to analyse slope gradient change at the junction of two first order channels to evaluate the effect of two different sources of debris-flow on one channel (Stock & Dietrich, 2006), considering that the two tributaries produce debris-flow at the same frequency.
Narrower constraints on α and β could also be obtained by obtaining more constraints on θ_{df}, through additional topographic analysis and better understanding its variability in relations to b and c_2. Interestingly, this requires studying debris-flow properties, and channel width and concavity evolution but does not require to constrain erosion rate and could thus be attempted in many more basins likely to be at steady-state. Such coupled analysis could also help reduce uncertainty on b and channel width evolution important for both DFIM and SPIM (DiBiase & Whipple, 2011; Lague, 2014; Neely & DiBiase, 2023).
Regarding k_{df} our observations yield a range of acceptable values anti-correlated to F_{df} which could be useful to guide future modeling studies. Physically, such scaling is consistent with the suggestion that in channels frequently scoured by debris flows the bedrock would have less time to weather in between events and thus be less erodible (Stock & Dietrich, 2006). Additional constraints on the model would benefit from a better understanding of the control and magnitude of F_{df}. Importantly, F_{df} likely increases with the frequency of extreme climatic event that may induce debris flows, such as wild-fire or intense rainfall, (Godt & Coe, 2007; Kean et al., 2011, 2013; DiBiase & Lamb, 2019). However, it is also likely that at landscape scale F_{df} increases with U, because of steeper hillslopes and more frequent landsliding. Thus further improvement of DFIM could be gained by constraining long-term debris flow frequency, whether from sedimentological archive or other proxies (Stoffel, 2010; Ballesteros-Cánovas et al., 2024), and connecting it to climate and tectonic conditions (Kiefer et al., 2021).

7 Conclusion

With a novel methodology for high resolution topography, we extracted all first order channels from a large compilation of steady state catchment with known erosion rates. We measured the initial gradient and concavity of these channels and found the former to increase as a power law of erosion rate and the latter to remain constant and positive across two order of magnitude of erosion rates. These observations agree with the prediction of an updated version of the debris-flow incision model (DFIM) from McGuire et al. (2023) in which we enforce that all sediments delivered by the hillslopes are transported by debris flows. Together, these observations determine optimal values for the exponent of the DFIM, $\alpha = 4.2 \pm 0.9$ and $\beta = 0.8 \pm 0.6$ with uncertainties dominated by the observed variability in concavity. Uncertainties may be halved if we only consider the variability of the mean concavity. Last, we provide first estimates of k_{df} as a function of F_{df} that would match observed morphology.

Although additional constraints on other parameters of the DFIM (e.g., c_2 and b), the controls on debris-flow frequency F_{df}, and on other aspect of the morphology (e.g., gradient reduction at channel junctions) are important challenges to address, the new insights on DFIM gained here pave the way for future studies with landscape evolution models (LEM) including DFIM. On the one hand the implications and prediction of existing 1D-LEM (McGuire et al., 2023) could be substantially refined by exploring a reduced parameter space. On the other hand, these constraints on the DFIM call for the development of new algorithm allowing to include DFIM in LEM, for example in models already including stochastic processes such as landslides (Campforts et al., 2020), with the potential to offer new insights on steepland topography and its dynamics.

8 Open Research

All the DEMs used are available online. The San Bernardino Mountains, San Gabriel Mountains and Oregon Coast Range basins are found on the OpenTopography website (Milodowski, 2014; Heimsath et al., 2019; DOGAMI, 2011). The Haute Provence basin comes from the RGE-alti©database (https://geoservices.ign.fr/rgealti) (IGN, 2014). Erosion rates are available online from the reported literature or the Octopus database (https://octopusdata.org/).

Acknowledgments

We are grateful to Vincent Godard for helping to access the IGN Lidar data, and Alexander Neely for stimulating discussions.

References

Ballesteros-Cánovas, J. A., Stoffel, M., de Haas, T., & Bodoque, J. M. (2024). Debris Flow Dating and Magnitude Reconstruction. In M. Jakob, S. McDougall, & P. Santi (Eds.), *Advances in Debris-flow Science and Practice* (pp. 219–248). Cham: Springer International Publishing. Retrieved 2024-10-08, from `https://doi.org/10.1007/978-3-031-48691-3_8` doi: 10.1007/978-3-031-48691-3_8

Benda, L., & Dunne, T. (1997). Stochastic forcing of sediment routing and storage in channel networks. *Wat. Resour. Res.*, *33*, 2865-2880.

Berhanu, M., Petroff, A., Devauchelle, O., Kudrolli, A., & Rothman, D. H. (2012). Shape and dynamics of seepage erosion in a horizontal granular bed. *Physical Review E*, *86*(4), 041304.

Binnie, S. A., Phillips, W. M., Summerfield, M. A., & Fifield, L. K. (2007, August). Tectonic uplift, threshold hillslopes, and denudation rates in a developing mountain range. *Geology*, *35*(8), 743–746. Retrieved 2014-07-29, from `http://geology.gsapubs.org/content/35/8/743` doi: 10.1130/G23641A.1

Campforts, B., Shobe, C. M., Steer, P., Vanmaercke, M., Lague, D., & Braun, J. (2020). HyLands 1.0: a hybrid landscape evolution model to simulate the impact of landslides and landslide-derived sediment on landscape evolution. *Geoscientific Model Dev.*, *13*(9), 3863-3886. doi: {10.5194/gmd-13-3863-2020}

Carretier, S., Martinod, P., Reich, M., & Goddéris, Y. (2016). Modelling sediment clasts transport during landscape evolution. *Earth Surf. Dynam.*, *4*, 237-251. doi: {10.5194/esurf-4-237-2016}

Codilean, A. T., Munack, H., Saktura, W. M., Cohen, T. J., Jacobs, Z., Ulm, S., . . . Panta, A. (2022, August). OCTOPUS database (v.2). *Earth System Science Data*, *14*(8), 3695–3713. Retrieved 2024-09-25, from `https://essd.copernicus.org/articles/14/3695/2022/` (Publisher: Copernicus GmbH) doi: 10.5194/essd-14-3695-2022

Davy, P., Croissant, T., & Lague, D. (2017). A precipiton method to calculate river hydrodynamics, with applications to flood prediction, landscape evolution models, and braiding instabilities. *J. Geophys. Res. Earth Surface*, *122*(8), 1491-1512. doi: {10.1002/2016JF004156}

Densmore, A., Ellis, M., & Anderson, R. (1998). Landsliding and the evolution of normal-fault-bounded mountains. *J. Geophys. Res.*, *103(B7)*, 15,203-15,219.

DiBiase, R. A., Heimsath, A. M., & Whipple, K. X. (2012, June). Hillslope response to tectonic forcing in threshold landscapes. *Earth Surface Processes and Landforms*, *37*(8), 855–865. Retrieved 2016-01-10, from `http://onlinelibrary.wiley.com/doi/10.1002/esp.3205/abstract` doi: 10.1002/esp.3205

DiBiase, R. A., & Lamb, M. P. (2019, December). Dry sediment loading of headwater channels fuels post-wildfire debris flows in bedrock landscapes. *Geology*, *48*(2), 189–193. Retrieved 2024-09-13, from `https://doi.org/10.1130/G46847.1` doi: 10.1130/G46847.1

DiBiase, R. A., & Whipple, K. X. (2011). The influence of erosion thresholds and runoff variability on the relationships among topography, climate, and erosion rate. *Journal of Geophysical Research: Earth Surface*, *116*(F4). Retrieved 2021-05-15, from `https://agupubs.onlinelibrary.wiley.com/doi/abs/10.1029/2011JF002095` (_eprint: https://agupubs.onlinelibrary.wiley.com/doi/pdf/10.1029/2011JF002095) doi: https://doi.org/10.1029/2011JF002095

DiBiase, R. A., Whipple, K. X., Heimsath, A. M., & Ouimet, W. B. (2010, January). Landscape form and millennial erosion rates in the San Gabriel Mountains, CA. *Earth and Planetary Science Letters*, *289*(1–2), 134–144. Retrieved 2014-03-07, from `http://www.sciencedirect.com/science/article/pii/S0012821X09006451` doi: 10.1016/j.epsl.2009.10.036

DOGAMI. (2011). *Oregon department of geology and mineral industries lidar program data. [dataset].* OpenTopography. Retrieved from `https://doi.org/10.5069/G9QC01D1` doi: 10.5069/G9QC01D1

Egholm, D. L., Knudsen, M. F., & Sandiford, M. (2013, June). Lifespan of mountain ranges scaled by feedbacks between landsliding and erosion by rivers. *Nature*, *498*(7455), 475–478. Retrieved 2017-09-12, from `https://www.nature.com/nature/journal/v498/n7455/full/nature12218.html` doi: 10.1038/nature12218

France-Lanord, C., & Derry, L. A. (1997). Organic carbon burial forcing of the carbon cycle from Himalaya erosion. *Nature*, *390*, 65-67.

Godard, V., Hippolyte, J.-C., Cushing, E., Espurt, N., Fleury, J., Bellier, O., . . . Team, t. A. (2020, April). Hillslope denudation and morphologic response to a rock uplift gradient. *Earth Surface Dynamics*, *8*(2), 221–243. doi: https://doi.org/10.5194/esurf-8-221-2020

Godt, J. W., & Coe, J. A. (2007, February). Alpine debris flows triggered by a 28 July 1999 thunderstorm in the central Front Range, Colorado. *Geomorphology*, *84*(1), 80–97. Retrieved 2024-10-08, from `https://www.sciencedirect.com/science/article/pii/S0169555X06002868` doi: 10.1016/j.geomorph.2006.07.009

Heimsath, A., Hudnut, M., K.and Lamb, & Whipple, K. (2019). *Mapping of san gabriel mountains, ca 2009 fire [dataset].* OpenTopography. Retrieved from `https://doi.org/10.5069/G94M92N4` doi: 10.5069/G94M92N4

Hergarten, S., Robl, J., & Stüwe, K. (2016). Tectonic geomorphology at small catchment sizes–extensions of the stream-power approach and the χ method. *Earth Surface Dynamics*, *4*(1), 1–9.

Hsu, L., Dietrich, W. E., & Sklar, L. S. (2008). Experimental study of bedrock erosion by granular flows. *Journal of Geophysical Research: Earth Surface*, *113*(F2). Retrieved 2021-11-08, from `https://onlinelibrary.wiley.com/doi/abs/10.1029/2007JF000778` (_eprint: https://onlinelibrary.wiley.com/doi/pdf/10.1029/2007JF000778) doi:

10.1029/2007JF000778
Hurst, M. D., Mudd, S. M., Attal, M., & Hilley, G. (2013, August). Hillslopes Record the Growth and Decay of Landscapes. *Science*, *341*(6148), 868–871. Retrieved 2020-09-09, from https://science.sciencemag.org/content/341/6148/868 doi: 10.1126/science.1241791
IGN. (2014). *Composante altimetrique du rge©[dataset].* Géoservices. Retrieved from https://geoservices.ign.fr/
Kean, J. W., McCoy, S. W., Tucker, G. E., Staley, D. M., & Coe, J. A. (2013). Runoff-generated debris flows: Observations and modeling of surge initiation, magnitude, and frequency. *Journal of Geophysical Research: Earth Surface*, *118*(4), 2190–2207.
Kean, J. W., Staley, D. M., & Cannon, S. H. (2011). In situ measurements of post-fire debris flows in southern California: Comparisons of the timing and magnitude of 24 debris-flow events with rainfall and soil moisture conditions. *Journal of Geophysical Research: Earth Surface*, *116*(F4). Retrieved 2024-10-08, from https://onlinelibrary.wiley.com/doi/abs/10.1029/2011JF002005 (_eprint: https://onlinelibrary.wiley.com/doi/pdf/10.1029/2011JF002005) doi: 10.1029/2011JF002005
Kiefer, C., Oswald, P., Moernaut, J., Fabbri, S. C., Mayr, C., Strasser, M., & Krautblatter, M. (2021, November). A 4000-year debris flow record based on amphibious investigations of fan delta activity in Plansee (Austria, Eastern Alps). *Earth Surface Dynamics*, *9*(6), 1481–1503. Retrieved 2024-10-08, from https://esurf.copernicus.org/articles/9/1481/2021/ (Publisher: Copernicus GmbH) doi: 10.5194/esurf-9-1481-2021
Kooi, H., & Beaumont, C. (1996). Large-scale geomorphology: Classical concepts reconciled and integrated with contemporary ideas via surface processes model. *J. Geophys. Res.*, *101*, 3361-3386.
Lague, D. (2014). The stream power river incision model: evidence, theory and beyond. *Earth Surface Processes and Landforms*, *39*(1), 38–61. Retrieved 2021-11-08, from https://onlinelibrary.wiley.com/doi/abs/10.1002/esp.3462 (_eprint: https://onlinelibrary.wiley.com/doi/pdf/10.1002/esp.3462) doi: 10.1002/esp.3462
Lague, D., & Davy, P. (2003). Constraints on the long-term colluvial erosion law by analyzing slope-area relationships at various tectonic uplift rates in the Siwaliks (Nepal). *J. Geophys. Res.*, *108(B2)*, 2129. doi: 10.1029/2002JB001893
Lurin, A., Marc, O., Meunier, P., & Carretier, S. (2023). A Robust Channel Head Extraction Method Based on High-Resolution Topographic Convergence, Suitable for Both Slowly and Fastly Eroding Landscapes. *Journal of Geophysical Research: Earth Surface*, *128*(9), e2022JF006999. Retrieved 2023-12-15, from https://onlinelibrary.wiley.com/doi/abs/10.1029/2022JF006999 (_eprint: https://onlinelibrary.wiley.com/doi/pdf/10.1029/2022JF006999) doi: 10.1029/2022JF006999
Marshall, J. A., Roering, J. J., Gavin, D. G., & Granger, D. E. (2017, May). Late Quaternary climatic controls on erosion rates and geomorphic processes in western Oregon, USA. *GSA Bulletin*, *129*(5-6), 715–731. Retrieved 2024-09-19, from https://doi.org/10.1130/B31509.1 doi: 10.1130/B31509.1
McCoy, S. W. (2012). *Controls on Erosion and Transport of Mass by Debris Flows* (PhD Thesis, University of Colorado, Boulder, Colorado USA). Retrieved from https://scholar.colorado.edu/concern/graduate_thesis_or_dissertations/4m90dv69g
McGuire, L. A., McCoy, S. W., Marc, O., Struble, W., & Barnhart, K. R. (2023, November). Steady-state forms of channel profiles shaped by debris flow and fluvial processes. *Earth Surface Dynamics*, *11*(6), 1117–1143. Retrieved 2024-01-09, from https://esurf.copernicus.org/articles/11/1117/2023/ (Publisher: Copernicus GmbH) doi: 10.5194/esurf-11-1117-2023

Milodowski, D. (2014). *Yucaipa ridge, san bernardino mountains, ca. [dataset].* OpenTopography. Retrieved from https://doi.org/10.5069/G93T9F55 doi: 10.5069/G93T9F55

Molnar, P., & England, P. (1990). Late Cenozoic uplift of mountain ranges and global climate change: chicken or egg? *Nature*, *346*, 29-34.

Montgomery, D. R., & Dietrich, W. E. (1988). Where do channels begin ? *Nature*, *336*, 231-233.

Mudd, S. M., & Furbish, D. J. (2005). Lateral migration of hillcrests in response to channel incision in soil-mantled landscapes. *Journal of Geophysical Research: Earth Surface*, *110*(F4). Retrieved 2024-10-03, from https://onlinelibrary.wiley.com/doi/abs/10.1029/2005JF000313 (_eprint: https://onlinelibrary.wiley.com/doi/pdf/10.1029/2005JF000313) doi: 10.1029/2005JF000313

Mudd, S. M., Harel, M.-A., Hurst, M. D., Grieve, S. W. D., & Marrero, S. M. (2016, August). The CAIRN Method: Automated, Reproducible Calculation of Catchment-Averaged Denudation Rates from Cosmogenic Nuclide Concentrations. *Earth Surface Dynamics*, *4*(3), 655–674. (Publisher: Copernicus GmbH) doi: 10.5194/esurf-4-655-2016

Neely, A. B., & DiBiase, R. A. (2023). Sediment controls on the transition from debris flow to fluvial channels in steep mountain ranges. *Earth Surface Processes and Landforms*, *48*(7), 1342–1361. Retrieved 2024-08-27, from https://onlinelibrary.wiley.com/doi/abs/10.1002/esp.5553 (_eprint: https://onlinelibrary.wiley.com/doi/pdf/10.1002/esp.5553) doi: 10.1002/esp.5553

Penserini, B. D., Roering, J. J., & Streig, A. (2017, April). A morphologic proxy for debris flow erosion with application to the earthquake deformation cycle, Cascadia Subduction Zone, USA. *Geomorphology*, *282*, 150–161. Retrieved 2021-11-08, from https://www.sciencedirect.com/science/article/pii/S0169555X16306821 doi: 10.1016/j.geomorph.2017.01.018

Perron, J. T., & Royden, L. (2013, May). An Integral Approach to Bedrock River Profile Analysis. *Earth Surface Processes and Landforms*, *38*(6), 570–576. doi: 10.1002/esp.3302

Prancevic, J. P., Lamb, M. P., & Fuller, B. M. (2014, 03). Incipient sediment motion across the river to debris-flow transition. *Geology*, *42*(3), 191-194. Retrieved from https://doi.org/10.1130/G34927.1 doi: 10.1130/G34927.1

Rickenmann, D. (1999, January). Empirical Relationships for Debris Flows. *Natural Hazards*, *19*(1), 47–77. Retrieved 2021-11-08, from https://doi.org/10.1023/A:1008064220727 doi: 10.1023/A:1008064220727

Roering, J. J., Perron, J. T., & Kirchner, J. W. (2007, December). Functional relationships between denudation and hillslope form and relief. *Earth and Planetary Science Letters*, *264*(1–2), 245–258. Retrieved 2014-08-01, from http://www.sciencedirect.com/science/article/pii/S0012821X07006061 doi: 10.1016/j.epsl.2007.09.035

Schwanghart, W., & Scherler, D. (2014). TopoToolbox 2 – MATLAB-based Software for Topographic Analysis and Modeling in Earth Surface Sciences. *Earth Surface Dynamics*, *2*, 1–7. doi: 10.5194/esurf-2-1-2014

Stock, J. D., & Dietrich, W. E. (2003). Valley incision by debris flows: Evidence of a topographic signature. *Water Resources Research*, *39*(4). Retrieved 2019-12-26, from https://agupubs.onlinelibrary.wiley.com/doi/abs/10.1029/2001WR001057 doi: 10.1029/2001WR001057

Stock, J. D., & Dietrich, W. E. (2006, September). Erosion of steepland valleys by debris flows. *GSA Bulletin*, *118*(9-10), 1125–1148. Retrieved 2017-12-05, from https://pubs.geoscienceworld.org/gsa/gsabulletin/article/118/9-10/1125/125333/erosion-of-steepland-valleys-by-debris-flows doi: 10.1130/B25902.1

Stoffel, M. (2010, March). Magnitude–frequency relationships of debris flows — A case study based on field surveys and tree-ring records. *Geomorphology*, *116*(1), 67–76. Retrieved 2024-10-08, from `https://www.sciencedirect.com/science/article/pii/S0169555X09004450` doi: 10.1016/j.geomorph.2009.10.009

Struble, W. T., McGuire, L. A., McCoy, S. W., Barnhart, K. R., & Marc, O. (2023). Debris-Flow Process Controls on Steepland Morphology in the San Gabriel Mountains, California. *Journal of Geophysical Research: Earth Surface*, *128*(7), e2022JF007017. Retrieved 2023-08-25, from `https://onlinelibrary.wiley.com/doi/abs/10.1029/2022JF007017` (_eprint: https://onlinelibrary.wiley.com/doi/pdf/10.1029/2022JF007017) doi: 10.1029/2022JF007017

Tucker, G. E., & Bras, R. L. (1998). Hillslope processes, drainage density, and landscape morphology. *Water resources research*, *34*(10), 2751–2764.

Tucker, G. E., & Hancock, G. R. (2010). Modelling landscape evolution. *Earth Surf. Proc. Land.*, *35*(1), 28-50. doi: {10.1002/esp.1952}

Whipple, K. X., Kirby, E., & Brocklehurst, H. (1999). Geomorphic limits to climate-induced increases in topographic relief. *Nature*, *401*, 39-43.

Willett, S. D., McCoy, S. W., Perron, J. T., Goren, L., & Chen, C.-Y. (2014). Dynamic Reorganization of River Basins. *Science*, *343*(6175), 1117+. doi: {10.1126/science.1248765}